Dissociative electron attachment to muonic hydrogen: $e+\mu p \rightarrow \mu+\mathrm{H}$

Kazuhiro Sakimoto
Institute of Space and Astronautical Science, Japan Aerospace Exploration Agency, Yoshinodai, Sagamihara 229-8510, Japan
(Received 27 August 2008; published 30 October 2008)

Rearrangement reaction in electron scattering from muonic hydrogen (μp) in highly excited states, i.e., $e+\mu p \rightarrow \mu+\mathrm{H}$, is theoretically investigated by using the R-matrix numerical method, recently developed by the present author [Phys. Rev. A **76**, 042513 (2007)]. This process can be identified as dissociative attachment (DA) if we use the terminology of molecular physics. The present study offers a rigorous treatment of the DA to the exotic system μp without introducing any type of decoupling approximation. The threshold behavior of the DA cross sections becomes peculiar because of the dipole interaction between e and μp and the degeneracy of the hydrogenic μp states.

DOI: 10.1103/PhysRevA.78.042509 PACS number(s): 36.10.Ee, 34.80.Ht, 36.10.Gv

I. INTRODUCTION

Research on the atomic and molecular systems involving antiprotons ($\bar{p}$) is very interesting in part because the antiprotons can be regarded as negative point charges much heavier than electrons. Above all, antiprotonic helium $\bar{p}\mathrm{He}^+$ is under recent intense study in this field. In describing the high orbital motion of $\bar{p}$-$\mathrm{He}^+(1s)$, we can find that a concept based on the Born-Oppenheimer (BO) separation is appropriate [1,2]. This exotic system shows some similarities to molecules. In the $\bar{p}$-H system, however, the situation becomes quite different because the electron is hardly bound at small $\bar{p}$-p distances, as evidenced by the presence of the so-called Fermi-Teller critical distance $R_{\mathrm{FT}}=0.639$ a.u. [3]. The molecular approach conventionally applied to low-energy heavy particle collisions is not useful in such a case. This was an obstacle to progress of the theoretical study, and it is only recent that a rigorous quantum-mechanical (QM) calculation has become possible for the $\bar{p}+\mathrm{H}$ collisions [4–6].

Muons (μ) are much lighter than antiprotons, but are still considered as heavy negative particles. The light μ mass makes an accurate QM treatment more feasible. Nevertheless, only a few QM calculations have been carried out so far also for the $\mu+\mathrm{H}$ collisions [7–9]. The purpose of the present study is to get a further understanding of the e-μ-p dynamics from a different aspect. Namely, we consider the inverse process of the μ capture by H, i.e.,

$$e+\mu p(N,L) \rightarrow \mu+\mathrm{H}(1s), \tag{1}$$

where the exotic atom μp is called muonic hydrogen, and (N,L) are the principal and angular momentum quantum numbers. When muons impinge on matter, the muonic hydrogen atoms are generally considered to form in high (N,L) states. The present study is restricted to such high-lying orbitals. This offers the numerical advantage that we can avoid treating the strong Coulomb attraction near the origin.

In molecular physics, a process such as Eq. (1) is known as dissociative attachment (DA). The research of DA to molecules has a long history [10]. As usually done in the DA study, we draw in Fig. 1 the potential energy curves of $\mu+p$ and $\mu+\mathrm{H}$ as a function of the relative distance R. The latter is the lowest 1σ adiabatic potential obtained by the BO approximation, which crosses at $R=R_{\mathrm{FT}}$ with the former, namely, the Coulomb potential. Figure 1 also shows the μp hydrogenic energy levels. We can see that the DA to the muonic hydrogen is an endoergic reaction if the principal quantum number of μp is $N\leqslant 13$. In most of the DA to molecules, electron resonances (i.e., temporally formed negative ions) in the fixed-nuclei picture are assumed to play a critical role [10,11]. In the present case, however, it is quite unlikely that the electron can be temporarily trapped at $R<R_{\mathrm{FT}}$. The DA to molecules can be treated by a nonresonance method [12], which directly takes account of the nonadiabatic effects leading to DA. In the $\mu+\mathrm{H}$ system, it has been found that the nonadiabatic coupling with electronic continua remains very strong even at μ-H distances twice as large as R_{FT} [8]. The adiabatic picture would be far from a good zeroth-order approximation for the understanding of the present DA dynamics.

In this paper, we present a rigorous QM treatment of the DA to the exotic system μp. The previous wave-packet propagation method used for the $\mu+\mathrm{H}$ collisions [7,8] is not

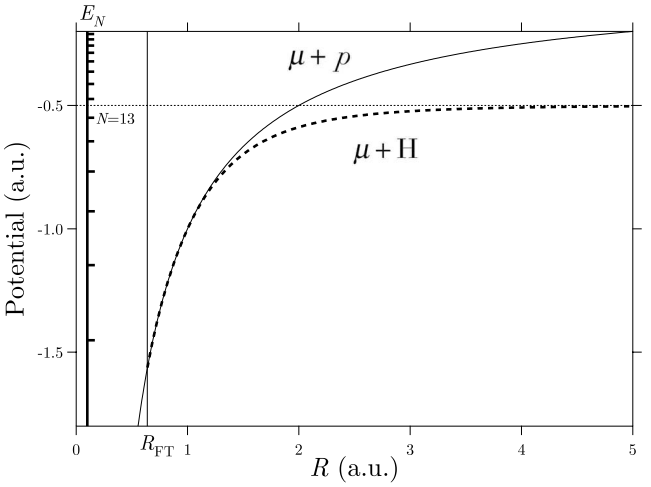

FIG. 1. The Coulomb potential of $\mu+p$ and the 1σ adiabatic (BO) potential of $\mu+\mathrm{H}$ as a function of the μ-p relative distance R. The μp hydrogenic energy levels E_N with the principal quantum number N are indicated on the left side of the figure. The energy corresponding to the dissociation limit $\mu+\mathrm{H}$ is −0.5 a.u. The vertical line labeled by R_{FT} represents the Fermi-Teller critical distance.

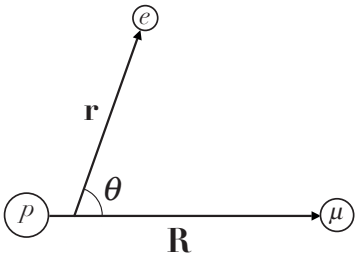

FIG. 2. Jacobi coordinates $(\mathbf{R},\mathbf{r})$ of the e-μ-p system.

appropriate if the kinetic energy in the dissociative channel μ+H is low as in the present case. The time-dependent method of Tong *et al.* [9] requires time-consuming computation for each collision energy. Here, we employ the R-matrix method recently developed by the present author for the $\bar{p}$ +He^+ collisions [13]. In the R-matrix method, once a matrix defined in the inner region is diagonalized, the scattering calculation at any energy can be accomplished easily. Instead, the inner-region computation is generally laborious. We consider the initial μp states $N=13$, 14, and 15, and low collision energies of electrons. Therefore, any electronic excited state of H is excluded as the asymptotic channel μ +H. In the present calculation, the nonrelativistic approximation is assumed, all the particles are considered to be pointlike, and the spin of the particles is omitted for simplicity.

II. SCATTERING THEORY

A. Scattering equation

Using the Jacobi coordinates $(\mathbf{R},\mathbf{r})$ shown in Fig. 2, the total Hamiltonian for the e-μ-p system can be written as

$$\tilde{H} = -\frac{1}{2m_R}\frac{\partial^2}{\partial R^2}R + \frac{\tilde{\mathbf{L}}^2}{2m_R R^2} - \frac{1}{2m_r}\frac{\partial^2}{\partial r^2}r + \frac{\tilde{\mathbf{l}}^2}{2m_r r^2} + V, \tag{2}$$

where m_R is the μ-p reduced mass, m_r is the e-μp reduced mass, $\tilde{\mathbf{L}}$ is the angular momentum vector (operator) of μ-p, and $\tilde{\mathbf{l}}$ is the electronic angular momentum vector. The interaction $V=V(R,r,\theta)$ is a function of R, r, and the angle θ between $\mathbf{R}$ and $\mathbf{r}$, and is explicitly given by

$$V = -\frac{1}{|(m_R/m_p)\mathbf{R}+\mathbf{r}|} + \frac{1}{|(m_R/m_\mu)\mathbf{R}-\mathbf{r}|} - \frac{1}{R}, \tag{3}$$

where m_p is the p mass, and m_μ is the μ mass. Here and in the following, we use atomic units unless otherwise stated.

The time-independent Schrödinger equation for the present system is

$$\tilde{H}\Psi_\tau^{JM\kappa}(\mathbf{R},\mathbf{r}) = E\Psi_\tau^{JM\kappa}(\mathbf{R},\mathbf{r}), \tag{4}$$

where E is the total energy, (J,M) are the total angular momentum quantum numbers, κ is the total parity, and τ indicates the initial scattering channel.

B. Scattering boundary conditions

For the incident channel $e+\mu p$, the total wave function $\Psi_\tau^{JM\kappa}$ can be given in the form

$$\Psi_\tau^{JM\kappa}(\mathbf{R},\mathbf{r}) = (Rr)^{-1}\sum_{NLl}\mathcal{Y}_{Ll}^{JM\kappa}(\hat{\mathbf{R}},\hat{\mathbf{r}})\Upsilon_{NL}(R)f_{NLl,\tau}^{J\kappa}(r). \tag{5}$$

The radial function $\Upsilon_{NL}(R)$ represents the bound state of the muonic hydrogen μp with the principal and angular momentum quantum numbers (N,L). The angular function $\mathcal{Y}_{Ll}^{JM\kappa}(\hat{\mathbf{R}},\hat{\mathbf{r}})$ is given by

$$\mathcal{Y}_{Ll}^{JM\kappa}(\hat{\mathbf{R}},\hat{\mathbf{r}}) = \sum_m (LM-m,lm|JM)Y_{LM-m}(\hat{\mathbf{R}})Y_{lm}(\hat{\mathbf{r}}), \tag{6}$$

where l is the electronic angular momentum quantum number, $Y_{LM-m}(\hat{\mathbf{R}})$ and $Y_{lm}(\hat{\mathbf{r}})$ are spherical harmonics, and $(LM-m,lm|JM)$ is a Clebsch-Gordan coefficient [14]. In the limit as $r\to\infty$, the scattering radial function $f_{NLl,\tau}^{J\kappa}(r)$ for the open channel (N,L,l) satisfies the boundary conditions

$$f_{NLl,\tau}^{J\kappa}(r) \sim s(\varepsilon,l;r)\delta_{NLl,\tau} + c(\varepsilon,l;r)\mathcal{K}_{NLl,\tau}^{J\kappa}, \tag{7}$$

where $\mathcal{K}_{NLl,\tau}^{J\kappa}$ is the scattering K-matrix element

$$s(\varepsilon,l;r) = \left(\frac{m_r}{2\pi k_N}\right)^{1/2}\sin(k_N r - l\pi/2), \tag{8}$$

$$c(\varepsilon,l;r) = \left(\frac{m_r}{2\pi k_N}\right)^{1/2}\cos(k_N r - l\pi/2), \tag{9}$$

and

$$\varepsilon = E - E_N = \frac{k_N^2}{2m_r}, \tag{10}$$

with the hydrogenic μp energy $E_N=-m_R/(2N^2)$.

If the distance R is larger than the range of the nonadiabatic coupling ($\simeq$1.5 a.u.), the adiabatic approximation is very good for the description of the μ+H state [8]. For the dissociative channel μ+H, therefore, the total wave function $\Psi_\tau^{JM\kappa}(\mathbf{R},\mathbf{r})$ at sufficiently large R can be given by [13]

$$\Psi_\tau^{JM\kappa}(\mathbf{R},\mathbf{r}) = (Rr)^{-1}\mathcal{D}_{M0}^{J\kappa}(\hat{\mathbf{R}})\chi_{1\sigma}(R;r,\theta)F_{1\sigma,\tau}^{J\kappa}(R), \tag{11}$$

where $\mathcal{D}_{M\lambda}^{J\kappa}(\hat{\mathbf{R}})$ is the parity-specified normalized Wigner's rotation matrix element related to the transformation from a space-fixed frame to a body-fixed (BF) frame in which the z axis is chosen along $\hat{\mathbf{R}}$: i.e., $\lambda=\tilde{J}_z=\tilde{l}_z$ ($\tilde{\mathbf{J}}=\tilde{\mathbf{L}}+\tilde{\mathbf{l}}$ being the total angular momentum vector), and $\chi_{1\sigma}(R;r,\theta)$ is the adiabatic wave function of the lowest 1σ state with the eigenenergy $E_{1\sigma}(R)$. The scattering radial function $F_{1\sigma,\tau}^{J\kappa}(R)$ can be expressed as

$$F_{1\sigma,\tau}^{J\kappa}(R) = S(E,J;R)\delta_{1\sigma,\tau} + C(E,J;R)\mathcal{K}_{1\sigma,\tau}^{J\kappa}, \tag{12}$$

where the functions $S(E,J;R)$ and $C(E,J;R)$ have the asymptotic forms

$$S(E,J;R) \sim \left[\frac{m_R}{2\pi K_{1\sigma}(R)}\right]^{1/2}\sin\left[\int^R K_{1\sigma}(R')dR'\right], \tag{13}$$

$$C(E,J;R) \sim \left[\frac{m_R}{2\pi K_{1\sigma}(R)}\right]^{1/2} \cos\left[\int^R K_{1\sigma}(R')dR'\right], \tag{14}$$

with

$$K_{1\sigma}(R) = \left\{2m_R\left[E - \frac{(J+1/2)^2}{2m_R R^2} - E_{1\sigma}(R)\right]\right\}^{1/2}. \tag{15}$$

The cross section for the DA to $\mu p(N,L)$ can be given by [15]

$$\sigma(N,L) = \frac{\pi}{k_N^2}\sum_{J\kappa}\frac{2J+1}{2L+1}\sum_l P^{J\kappa}(N,L,l), \tag{16}$$

with the DA probability

$$P^{J\kappa}(N,L,l) = |\mathcal{S}^{J\kappa}_{1\sigma,NLl}|^2, \tag{17}$$

where $\mathcal{S}^{J\kappa}_{1\sigma,NLl}$ is the scattering S-matrix element for the $\tau=(N,L,l)\rightarrow 1\sigma$ transition. Because the dissociative channel is the 1σ state, only the parity of $\kappa=(-1)^J$ is allowed in the present DA process.

C. *R*-matrix method

The present treatment of the scattering calculation is based on the R-matrix method [16,17] using the nonuniform boundary condition [18]. Here, only its outline is given. For the details of the numerical method, see Ref. [13].

We consider the eigenvalue equation

$$[\tilde{H} + \tilde{L}_B]\Phi_\rho^{JM\kappa}(\mathbf{R},\mathbf{r}) = E_\rho^{J\kappa}\Phi_\rho^{JM\kappa}(\mathbf{R},\mathbf{r}), \tag{18}$$

where

$$\tilde{L}_B = \frac{1}{2m_R A}\delta(R-A)\frac{\partial}{\partial R}R + \frac{1}{2m_r a}\delta(r-a)\frac{\partial}{\partial r}r \tag{19}$$

is the Bloch operator [19], and $(R=A, r=a)$ is the boundary defining the inner region. The wave function $\Phi_\rho^{JM\kappa}(\mathbf{R},\mathbf{r})$ can be normalized to unity, i.e.,

$$\langle\Phi_\rho^{JM\kappa}|\Phi_{\rho'}^{JM\kappa}\rangle_{A,a} = \delta_{\rho,\rho'}, \tag{20}$$

where the subscript A, a indicates that the integral range for R and r is limited to the inner region. We can expand the R-matrix wave function $\Phi_\rho^{JM\kappa}$ each near the boundary line as

$$\Phi_\rho^{JM\kappa}(\mathbf{R},\mathbf{r}) = (Rr)^{-1}\mathcal{D}^{J\kappa}_{M0}(\hat{\mathbf{R}})\chi_{1\sigma}(R;r,\theta)H^{J\kappa}_{1\sigma,\rho}(R) \tag{21}$$

for $R\sim A$ and

$$\Phi_\rho^{JM\kappa}(\mathbf{R},\mathbf{r}) = (Rr)^{-1}\sum_{NLl}\mathcal{Y}^{JM\kappa}_{Ll}(\hat{\mathbf{R}},\hat{\mathbf{r}})\Upsilon_{NL}(R)h^{J\kappa}_{NLl,\rho}(r), \tag{22}$$

for $r\sim a$. Then, the R-matrix elements can be given by [16]

$$\mathcal{R}^{J\kappa}_{1\sigma,1\sigma} = \frac{1}{2m_R}\sum_\rho\frac{[H^{J\kappa}_{1\sigma,\rho}(A)]^2}{E_\rho^{J\kappa}-E}, \tag{23}$$

$$\mathcal{R}^{J\kappa}_{NLl,N'L'l'} = \frac{1}{2m_r}\sum_\rho\frac{h^{J\kappa}_{NLl,\rho}(a)h^{J\kappa}_{N'L'l',\rho}(a)}{E_\rho^{J\kappa}-E}, \tag{24}$$

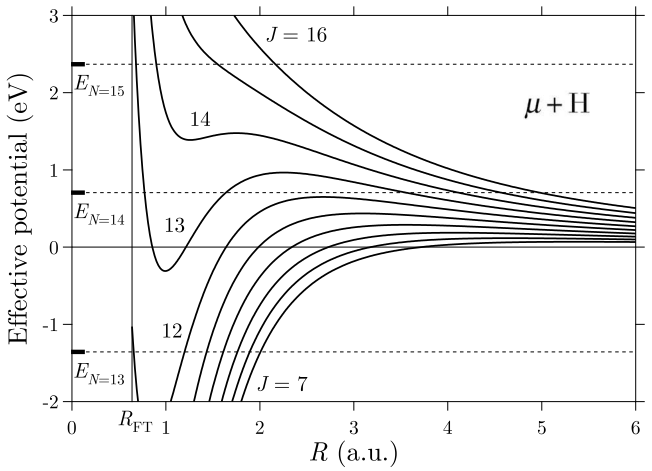

FIG. 3. Effective potential $V_{\rm eff}(R)$ of the dissociative channel μ+H (the sum of the centrifugal and 1σ adiabatic potentials) as a function of R for $J=7-16$. The energies are measured from the dissociation limit. The vertical line labeled by $R_{\rm FT}$ represents the Fermi-Teller critical distance. The μp hydrogenic energy levels E_N are shown for $N=13$, 14, and 15.

$$m_R\mathcal{R}^{J\kappa}_{NLl,1\sigma} = m_r\mathcal{R}^{J\kappa}_{1\sigma,NLl} = \frac{1}{2}\sum_\rho\frac{h^{J\kappa}_{NLl,\rho}(a)H^{J\kappa}_{1\sigma,\rho}(A)}{E_\rho^{J\kappa}-E}. \tag{25}$$

The scattering K and S matrices can be calculated from the R matrix in the usual way [21].

To numerically solve the R-matrix eigenvalue equation (18), we expand the wave function $\Phi_\rho^{JM\kappa}$ in the BF frame as [13]

$$\Phi_\rho^{JM\kappa}(\mathbf{R},\mathbf{r}) = (Rr)^{-1}\sum_{\lambda\geq 0}\mathcal{D}^{J\kappa}_{M\lambda}(\hat{\mathbf{R}})\varphi_\rho^{J\kappa\lambda}(R,r,\theta). \tag{26}$$

The function $\varphi_\rho^{J\kappa\lambda}(R,r,\theta)$ is calculated by using direct numerical solution based on the grid representation [13]. The amplitudes $H^{J\kappa}_{1\sigma,\rho}(A)$ and $h^{J\kappa}_{NLl,\rho}(a)$ needed in Eqs. (23)–(25) can be obtained by

$$H^{J\kappa}_{1\sigma,\rho}(A) = \langle\chi_{1\sigma}|\varphi_\rho^{J\kappa\lambda=0}\rangle|_{R=A}, \tag{27}$$

$$h^{J\kappa}_{NLl,\rho}(a) = \sum_{\lambda\geq 0}U^{J\kappa l}_{L\lambda}\langle\mathcal{P}_l^\lambda\Upsilon_{NL}|\varphi_\rho^{J\kappa\lambda}\rangle|_{r=a}, \tag{28}$$

where $\mathcal{P}_l^\lambda(\cos\theta)=\sqrt{2\pi}Y_{l\lambda}(\theta,0)$ is normalized to unity, and

$$U^{J\kappa l}_{L\lambda} = \left(\frac{2L+1}{2J+1}\right)^{1/2}(L0,l\lambda|J\lambda)\frac{1+\kappa(-1)^{L+l}}{[2(1+\delta_{\lambda,0})]^{1/2}}. \tag{29}$$

D. Numerical calculations

The scattering calculations were carried out for the initial states $N=13$, 14, and 15. Figure 3 shows the energies E_N of these states and the effective potential $V_{\rm eff}(R)$ for the μ+H motion, calculated from the 1σ adiabatic potential. The DA channel becomes open when the total energy is $E=\varepsilon+E_N > E_{1\sigma}(\infty)$. In the present case ($N\leq 15$ and $L\geq 10$), the $\mu+p$ motion is localized in the area of $R\leq 2.0$ a.u. This means that the DA is forbidden unless the μ+H scattering wave function has a finite amplitude at $R\leq 2.0$ a.u.

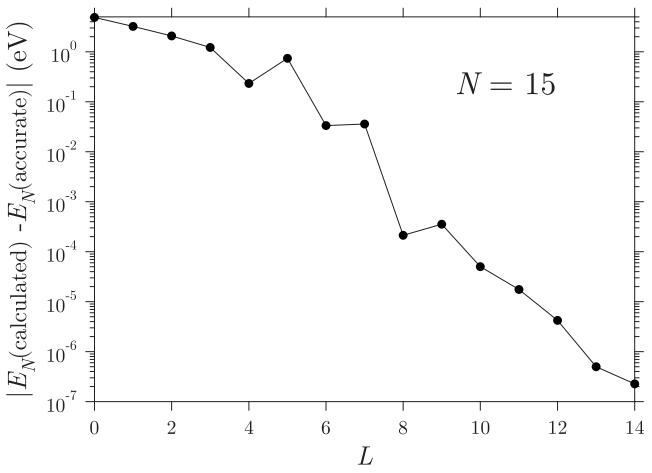

FIG. 4. The deviation of the μp energies calculated using the grid of N_R=30 from the accurate value $-m_R/(2N^2)$ for N=15 and L=0–14.

We took the boundary values A=3 a.u. and a=10 a.u., and included the λ=0 and 1 states in the inner-region calculation. We checked the convergence of the inner-region calculation with respect to the numbers of grid points (N_R, N_r, N_θ) in the (R, r, θ) coordinate space, as done in Ref. [13]. The results shown below were calculated by adopting a set (N_R, N_r, N_θ)=(30,35,10), which gave the error of the transition probabilities less than 1%. Figure 4 shows the deviation of the μp energies obtained in the present grid calculation (N_R=30) from the accurate value $-m_R/(2N^2)$ for N=15. We can see that the calculated energies are less accurate for lower L. This is because the minimum of the effective potential of $\mu+p$ becomes deeper as L decreases. The incident electrons having the angular momenta $l>2$ contribute negligibly to the DA. (In the present calculation, l=0–4 are included.) Therefore, as long as high initial L states are considered, the poor accuracy for the low L states does not matter.

In order to calculate the functions $S(E,J;R)$ and $C(E,J;R)$ at $R=A$ in Eq. (12), the asymptotic solutions (13) and (14) are numerically propagated backward from a sufficiently large distance R. To eliminate the long-range dipole coupling effect in the $e+\mu p$ channel, we propagated the R matrix from $r=a$ to a large distance $r=r_{\max}$ [13,20]. For the calculation of the DA probabilities, $r_{\max}$=100 a.u. was chosen unless otherwise stated. (For the convergence of the DA probabilities with respect to $r_{\max}$, Fig. 13 serves as a reference.)

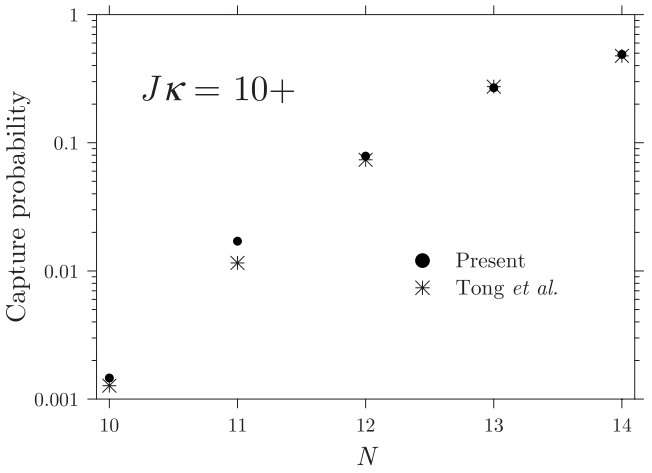

FIG. 5. Probabilities of the μ capture into $\mu p(N)$ in the μ+H collisions for $J\kappa$=10+ at the μ+H collision energy $T=E-E_{1\sigma}(\infty)$ =2.0 eV. The present results are compared with those of Tong *et al.* [9].

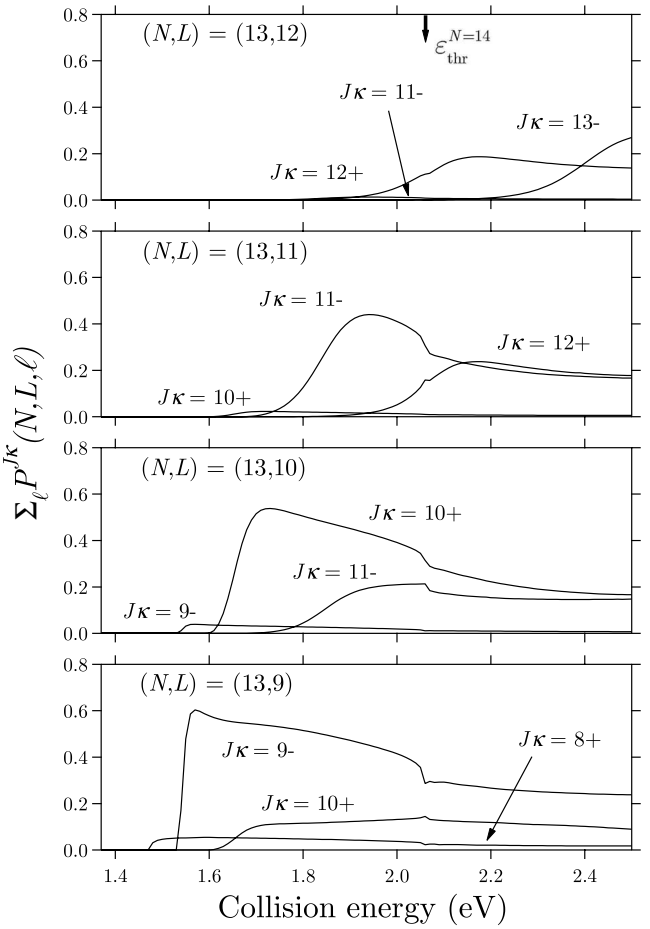

FIG. 6. The sum of the DA probabilities $P^{J\kappa}(N,L,l)$ over l for the initial state N=13 as a function of the electron collision energy $\varepsilon=E-E_{N=13}$. $\varepsilon_{\text{thr}}^{N=14}=E_{N=14}-E_{N=13}$ is the threshold for the N=14 excitation.

In the time-dependent QM calculation, fortunately Tong *et al.* [9] present the N-specified probabilities of μ+H $\rightarrow \mu p(N)+e$ at a low energy, which can be directly compared with the present calculation. The result of the comparison, shown in Fig. 5, seems to be acceptable.

III. RESULTS AND DISCUSSION

A. DA probabilities and cross sections

The results of the DA probabilities $\Sigma_l P^{J\kappa}(N,L,l)$ for the initial state N=13 are shown as a function of the electron collision energy ε in Fig. 6. The DA reaction for N=13 is endoergic, and has the threshold energy $\varepsilon_{\text{thr}}^{\text{DA}}=E_{1\sigma}(\infty)-E_{N=13}$=1.356 eV. If we look at each partial wave specified by J, however, the effective DA threshold would be larger

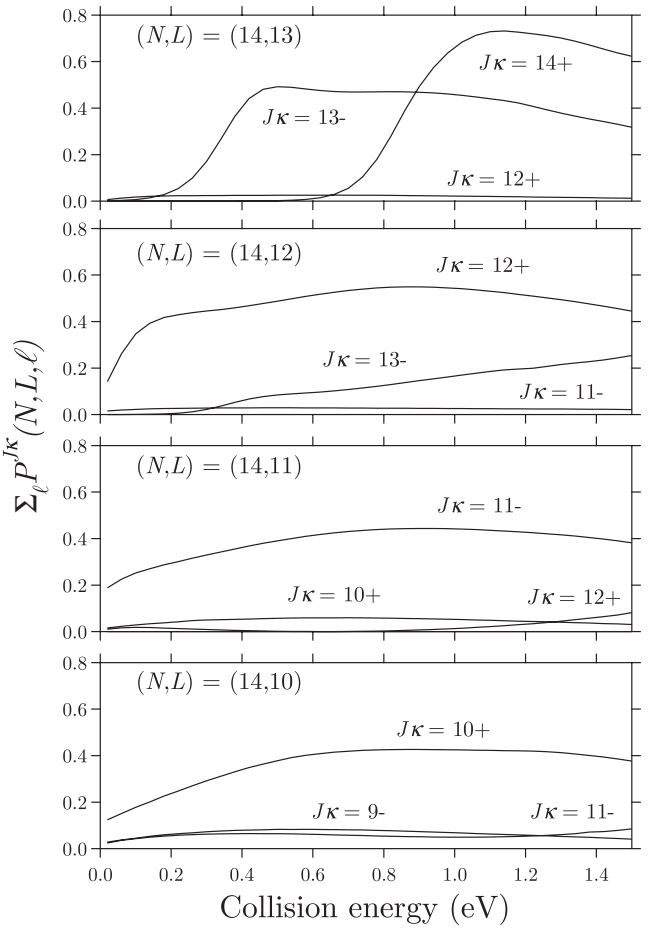

FIG. 7. The sum of the DA probabilities $P^{J\kappa}(N,L,l)$ over l for the initial state $N=14$ as a function of the electron collision energy $\varepsilon=E-E_{N=14}$.

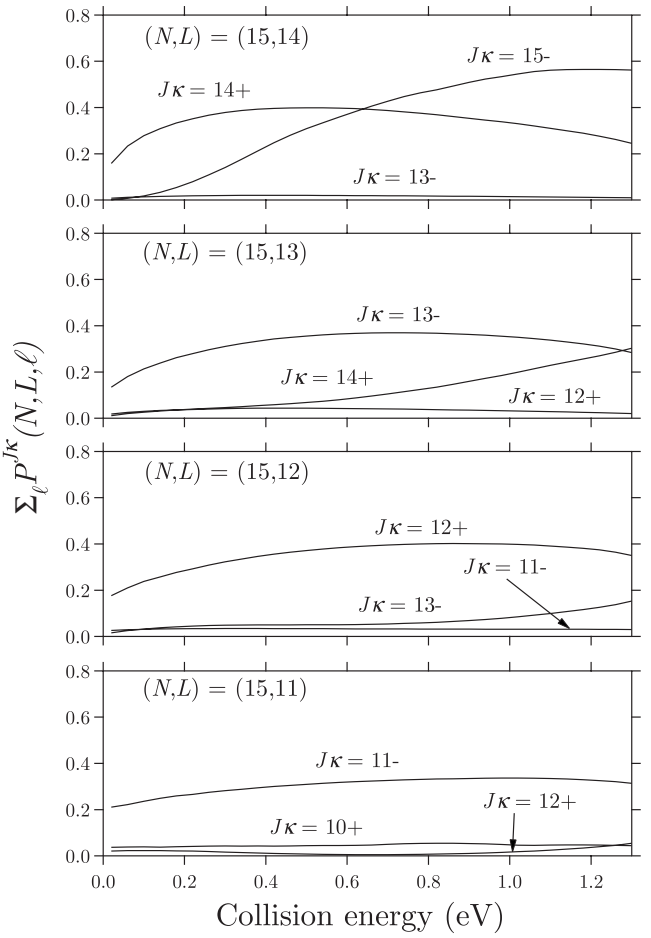

FIG. 8. The sum of the DA probabilities $P^{J\kappa}(N,L,l)$ over l for the initial state $N=15$ as a function of the electron collision energy $\varepsilon=E-E_{N=15}$.

than $\varepsilon_{\rm thr}^{\rm DA}$ because of the centrifugal barrier of the dissociative channel μ+H. The interaction range $R_{\rm int}$ for the rearrangement reaction (1) is estimated to be $R_{\rm int}\simeq 1.5$ a.u. from the study of the μ capture by H [8]. Figure 3 shows that the local maximum of the effective potential $V_{\rm eff}(R)$ for $J\leqslant 14$ is always located at a distance (e.g., =1.75 a.u. for $J=14$) larger than $R_{\rm int}$. Therefore, the effective DA threshold can be given by the barrier height of $V_{\rm eff}(R)$ if $J\leqslant 14$. For the initial state $N\geqslant 14$ (Figs. 7 and 8), the DA reaction is exoergic, and is allowed at all the electron energies ε if $J\leqslant 12$ ($N=14$) or if $J\leqslant 14$ ($N=15$), as can be expected from Fig. 3. If $N=15$ and $J=15$, the radial turning point $R_{\rm TP}$ of the μ+H motion, estimated from $V_{\rm eff}(R)$, is slightly larger than $R_{\rm int}$ at $\varepsilon=0$, and accordingly the DA probability becomes very small as $\varepsilon\rightarrow 0$. In all the cases shown here, the DA probabilities are very small ($\lesssim 10^{-3}$) if J takes the values of $|J-L|\geqslant 2$. This is because only the electrons with the low angular momentum $l=0$ or 1 can sufficiently approach μp at low energies.

The DA cross sections $\sigma(N,L)$ for the initial states $N=13$, 14, and 15 are shown in Figs. 9–11, respectively. Especially for $N=13$ and also for $(N,L)=(14,13)$, because the DA probabilities are rapidly rising as the energy increases from the J-dependent effective threshold, the DA cross sections have complicated energy dependence. For the other initial states, in contrast, the cross sections are monotonically decreasing with ε.

The muonic hydrogen μp in high N states is also considered as a typical dipole. Because of the degeneracy of the

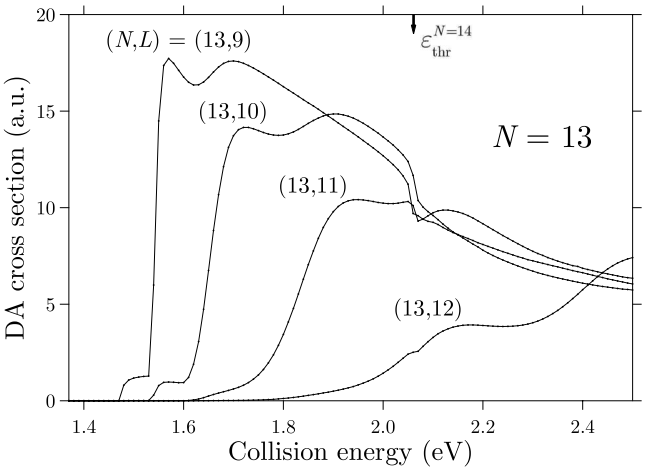

FIG. 9. DA cross sections $\sigma(N,L)$ for the initial state $N=13$ as a function of the electron collision energy $\varepsilon=E-E_{N=13}$. $\varepsilon_{\rm thr}^{N=14}=E_{N=14}-E_{N=13}$ is the threshold for the $N=14$ excitation.

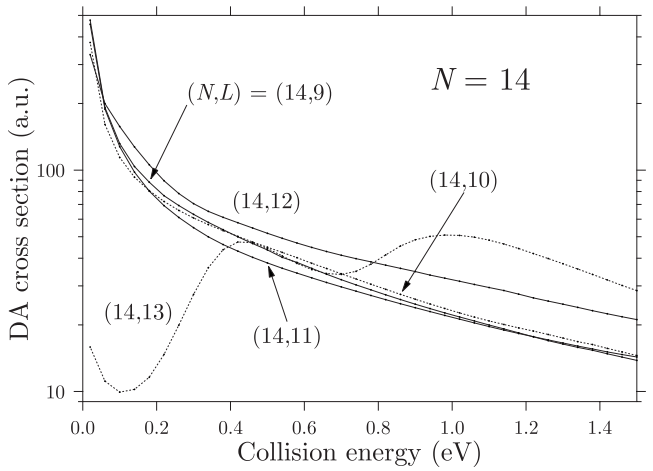

FIG. 10. DA cross sections $\sigma(N,L)$ for the initial state $N=14$ as a function of the electron collision energy $\varepsilon=E-E_{N=14}$.

hydrogenic states, the $e+\mu p$ system effectively has an asymptotic dipole potential still proportional to r^{-2} (i.e., the linear Stark effect) [22]. Then, it becomes probable that the effective long-range dipole force becomes attractive, and overcomes the centrifugal repulsion. This causes some interesting phenomena [23–25], which will be discussed in the next section.

B. Effects of dipole interaction

In the limit as $r\to\infty$, the sum of the centrifugal potential and the interaction (3) becomes

$$\frac{\tilde{\mathbf{l}}^2}{2m_r r^2}+V\to\frac{\tilde{\mathbf{l}}^2+2m_r R\cos\theta}{2m_r r^2}-\frac{1}{R}. \tag{30}$$

For each fixed N, we diagonalize the matrix elements defined by [22,25]

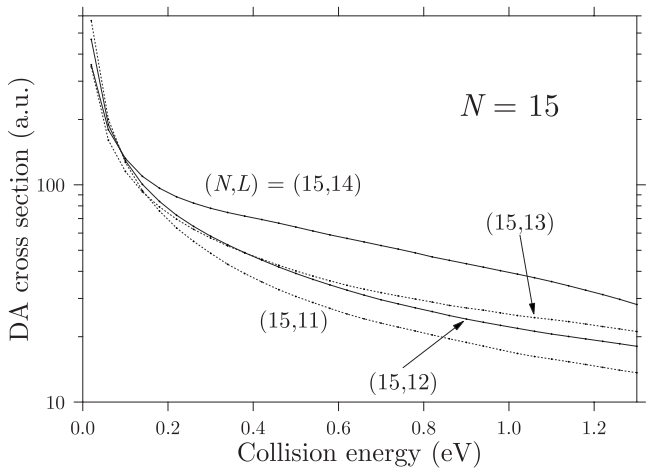

FIG. 11. DA cross sections $\sigma(N,L)$ for the initial state $N=15$ as a function of the electron collision energy $\varepsilon=E-E_{N=15}$.

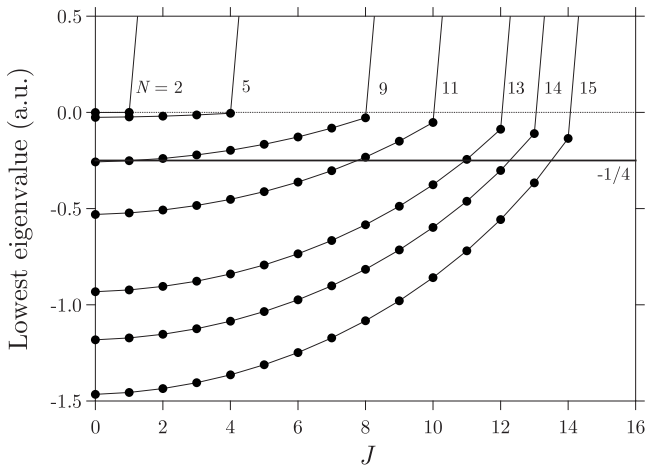

FIG. 12. The lowest eigenvalue $\Lambda_{\alpha=1}^{J\kappa N}$ as a function of the total angular momentum J for $\kappa=(-1)^J$ and $N=2-15$.

$$(\mathcal{Y}_{Ll}^{JM\kappa}\Upsilon_{NL}|\tilde{\mathbf{l}}^2+2m_r R\cos\theta|\mathcal{Y}_{L'l'}^{JM\kappa}\Upsilon_{NL'}), \tag{31}$$

and denote the eigenvalues by $\Lambda_\alpha^{J\kappa N}$ with $\alpha=1,2,\ldots$. Then, the Hamiltonian (2) at large r can be reduced to

$$\bar{H}_{\rm asym}=-\frac{1}{2m_r r}\frac{\partial^2}{\partial r^2}r+\frac{\Lambda_\alpha^{J\kappa N}}{2m_r r^2}+E_N. \tag{32}$$

Therefore, the potential for the electron radial motion at large r is given by $\Lambda_\alpha^{J\kappa N}/(2m_r r^2)$ and not simply by $l(l+1)/(2m_r r^2)$. If $\Lambda_\alpha^{J\kappa N}<-1/4$, the situation becomes exactly the same as that holding in the presence of the Coulomb attraction: the tail of the potential $\Lambda_\alpha^{J\kappa N}/(2m_r r^2)$ supports an infinite number of bound states [26] and furthermore the transition probability of the collisional excitation differs from zero in the vicinity of the excitation threshold [23,24].

Figure 12 shows the lowest eigenvalue $\Lambda_{\alpha=1}^{J\kappa N}$ as a function of the total angular momentum J for $N=2-15$. If $N=14$, $\Lambda_{\alpha=1}^{J\kappa N}$ is only slightly less than $-1/4$ for $J=12$, and becomes more negative as J decreases. Accordingly, we can see that the DA probabilities $\Sigma_l P^{J\kappa}(N,L,l)$ especially for $N=13$ and $J\leqslant 11$ (Fig. 6) have the anomalies at the $N=14$ excitation threshold $\varepsilon_{\rm thr}^{N=14}=E_{N=14}-E_{N=13}=2.061$ eV, and furthermore the DA probabilities for $N=14$ and $J\leqslant 12$ and for $N=15$ and $J\leqslant 14$ (Figs. 7 and 8) remain finite at zero energy $\varepsilon=0$. Because of the finite probability at $\varepsilon=0$, the DA cross section diverges as ε^{-1} in the limit of zero electron energy (Figs. 10 and 11). This behavior is quite different from the zero-energy limit ($\propto\varepsilon^{-1/2}$) in the DA to ordinary molecules [10].

Detailed behavior of the DA probabilities in the neighborhood of $\varepsilon=0$ is shown in Fig. 13 for $(N,L)=(14,11)$ and (14, 12). In the numerical calculation, $r_{\rm max}$ must be taken larger as ε decreases. The figure also includes the results obtained by further choosing $r_{\rm max}=150$ and 200 a.u. We can see that a much larger value of $r_{\rm max}$ is needed if the energy is $\varepsilon<5\times10^{-3}$ eV. It should be mentioned furthermore that an accurate calculation of the probabilities is still more difficult at energies very near $\varepsilon=0$ also because of the limited accuracy of the μp energy levels. Figure 4 implies that, for example,

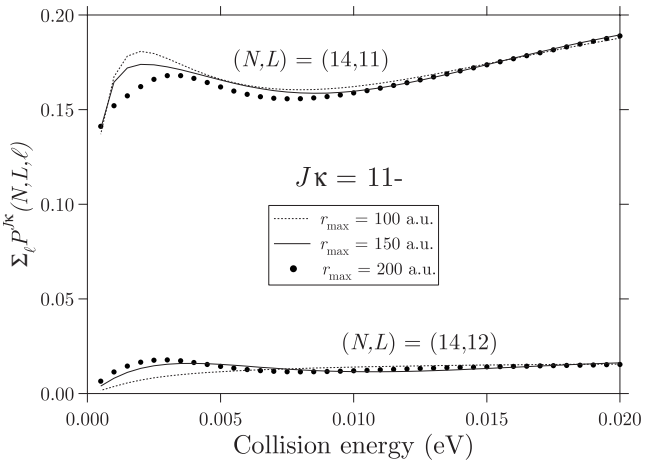

FIG. 13. The sum of the DA probabilities $P^{J\kappa}(N,L,l)$ over l for $J\kappa=11-$ and $N=14$ in the neighborhood of the electron collision energy $\varepsilon=E-E_{N=14}=0$, obtained by choosing $r_{\max}=100$, 150, and 200 a.u.

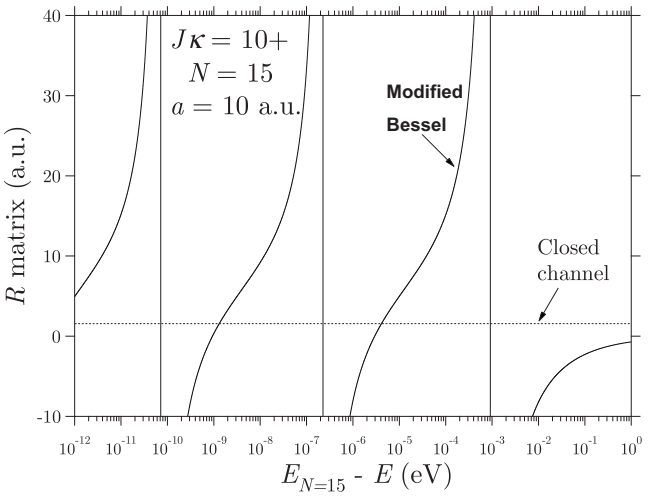

FIG. 14. The diagonal R-matrix element for $J\kappa=10+$, $N=15$, and $a=10$ a.u. as a function of the energy $E_{N=15}-E$ (>0), obtained by the physical solution $g(r)/r$ expressible in terms of the modified Bessel function and by the numerical calculation for the transformed closed channel α.

the electron energies of $\varepsilon \lesssim 10^{-4}$ eV have no physical meaning for $(N,L)=(15,10)$ in the present calculation.

Resonances are of special significance in the e-$\bar{p}$-He^{2+} system. Originally, the antiprotonic helium $\bar{p}He^{+}$ can be observed only as resonance states [1]. In the $\bar{p}+He^{+}$ collisions, it has been further found that the $\bar{p}$ capture probability shows a saw-edged structure owing to the overcrowding of the $\bar{p}He^{+}$ resonances, and the resonance process makes a dominant contribution to the $\bar{p}$ capture [13,27]. A huge number of the resonances originate from the long-range Coulomb attraction inherent in each of the rearrangement channels. How does the situation change for the e-μ-p system? The fact that the potential $\Lambda_{\alpha}^{J\kappa N}/(2m_r r^2)$ can support the bound states bears mathematical evidence of the existence of $(e\mu p)^{-}$ resonances. The physical solution $g(r)/r$ for the Hamiltonian (32) which decays to zero at infinity is given in terms of a modified Bessel function [22,25]. As done by Shimamura [25], we can roughly estimate the resonance energy positions by setting

$$g(a)\left[\frac{dg(a)}{dr}\right]^{-1} = \mathcal{R}^{J\kappa}_{N\alpha,N\alpha}, \tag{33}$$

where $\mathcal{R}^{J\kappa}_{N\alpha,NL\alpha}$ is the diagonal element of the R matrix for the transformed $(N,L,l \Rightarrow N,\alpha)$ closed channel at $r=a$. Figure 14 shows a typical example, related to the Feshbach resonances $[e\text{-}\mu p(N=15)]^{**}$ (i.e., $E=\varepsilon+E_{N=14}<E_{N=15}$), and implies that the resonances appear in a narrow range of energies just below the $N=15$ excitation threshold $\varepsilon_{\rm thr}^{N=15}$ (i.e., $|E-E_{N=15}|<10^{-5}$ eV). In order to properly describe these resonances, the accuracy of the calculated excitation energies must be better than the energy difference $|E-E_{N=15}|$. However, Fig. 4 shows that the desired accuracy achieves only for $L \geqslant 12$. Therefore, the present calculation is not appropriate for the investigation of these resonances. In fact, efforts to find out the resonances (also associated with other excitation energies E_N) failed in the present study. In any case, because the resonances exist only in the localized areas, we can conclude that the resonances are insignificant at these low energies. In the present case, $\Lambda_{\alpha=1}^{J\kappa N} \sim -1.5$ a.u. at minimum. If $\Lambda_{\alpha=1}^{J\kappa N}$ took a much more negative value ($\ll -1$ a.u.), the resonances would be located at energies far below the excitation threshold, and could be detected in the present numerical study.

If we consider the resonances characterized as $[\mu\text{-H}(n=2)]^{**}$ with n being the principal quantum number of the hydrogen, the lowest eigenvalue of the corresponding centrifugal and dipole matrix elements becomes $\Lambda \simeq -1000$ a.u. for $J=10$. As discussed by Shimamura [25], prominent resonances could be easily found in such a case. However, these resonances appear at energies much higher than those considered in this study.

IV. SUMMARY

The R-matrix method, developed by the present author [13], is applied to the DA to muonic hydrogen. The dipole interaction between e and μp and the hydrogenic degeneracy of μp produce the peculiarities in the DA cross section, and further support resonances just below the μp excitation energies. Unfortunately, no such resonances could be found in the present calculation. For a resonance search at low energies, the numerical computation with much higher accuracy is needed though it becomes extremely laborious. This rather ensures that the contribution of these resonances is negligible in the DA to μp. As a process similar to the present exotic DA, we can consider $e+\bar{p}He^{2+} \rightarrow \bar{p}+He^{+}$, which may be identified as dissociative recombination (DR). It is expected in this case that the resonances are significant, and play a dominant role [27]. The application of the present R-matrix method to this DR process is very interesting, and will be reported in the near future.

ACKNOWLEDGMENTS

The author would like to thank to Professor I. Shimamura for valuable discussion. The present work was partially supported by the Grant-in-Aid for Scientific Research from the Ministry of Education, Science, Sports, and Technology of Japan.

[1] T. Yamazaki *et al.*, Phys. Rep. **366**, 183 (2002).
[2] I. Shimamura, Phys. Rev. A **46**, 3776 (1992).
[3] E. Fermi and E. Teller, Phys. Rev. **72**, 399 (1947).
[4] K. Sakimoto, Phys. Rev. A **65**, 012706 (2001).
[5] K. Sakimoto, Phys. Rev. A **70**, 064501 (2004).
[6] X. M. Tong, K. Hino, and N. Toshima, Phys. Rev. Lett. **97**, 243202 (2006).
[7] K. Sakimoto, J. Phys. B **35**, 997 (2002).
[8] K. Sakimoto, Phys. Rev. A **66**, 032506 (2002).
[9] X. M. Tong, T. Shirahama, K. Hino, and N. Toshima, Phys. Rev. A **75**, 052711 (2007).
[10] A. Chutjian, A. Garscadden, and J. M. Wadehra, Phys. Rep. **264**, 393 (1996).
[11] I. I. Fabrikant, J. M. Wadehra, and Y. Xu, Phys. Scr., T **T96**, 45 (2002).
[12] D. Rabli and M. A. Morrison, Phys. Rev. Lett. **97**, 013201 (2006).
[13] K. Sakimoto, Phys. Rev. A **76**, 042513 (2007).
[14] M. E. Rose, *Elementary Theory of Angular Momentum* (Wiley, New York, 1957).
[15] H. Takagi, J. Phys. B **26**, 4815 (1993).
[16] P. G. Burke and W. D. Robb, Adv. At. Mol. Phys. **11**, 143 (1975).
[17] M. LeDourneuf, B. I. Schneider, and P. G. Burke, J. Phys. B **12**, L365 (1979).
[18] D. Baye *et al.*, J. Phys. B **31**, 3439 (1998).
[19] C. Bloch, Nucl. Phys. **4**, 503 (1957).
[20] K. L. Baluja, P. G. Burke, and L. A. Morgan, Comput. Phys. Commun. **27**, 299 (1982).
[21] K. A. Berrington *et al.*, J. Phys. B **20**, 6379 (1987).
[22] M. J. Seaton, Proc. Phys. Soc. London **77**, 174 (1961).
[23] M. Gailitis and R. Damburg, Proc. Phys. Soc. London **82**, 192 (1963).
[24] T. F. O'Malley, Phys. Rev. **137**, A1668 (1965).
[25] I. Shimamura, Phys. Rev. A **40**, 4863 (1989).
[26] L. D. Landau and E. M. Lifshitz, *Quantum Mechanics*, 3rd ed. (Pergamon, Oxford, 1977), Sec. 35.
[27] K. Sakimoto, Phys. Rev. A **74**, 022709 (2006).